ISSN 1674-1056
http://cpb.iphy.ac.cn
http://iopscience.iop.org/cpb
中国物理 B
Chinese Physics
中国物理 Chinese Physics B

Interfacial effect on the reverse of magnetization and ultrafast demagnetization in Co/Ni bilayers with perpendicular magnetic anisotropy

Zi-Zhao Gong(弓子召), Wei Zhang(张伟), Wei He(何为), Xiang-Qun Zhang(张向群), Yong Liu(刘永), Zhao-Hua Cheng(成昭华)
Citation: Chin. Phys. B . 2018, 27(5): 057501. **doi:** 10.1088/1674-1056/27/5/057501

Journal homepage: http://cpb.iphy.ac.cn; http://iopscience.iop.org/cpb

What follows is a list of articles you may be interested in

Effects of dipolar interactions on magnetic properties of Co nanowire arrays

Hong-Jian Li(李洪健), MingYue(岳明), Qiong Wu(吴琼), Yi Peng(彭懿), Yu-Qing Li(李玉卿), Wei-Qiang Liu(刘卫强), Dong-Tao Zhang(张东涛), Jiu-Xing Zhang(张久兴)
Chin. Phys. B . 2017, 26(11): 117503. **doi:** 10.1088/1674-1056/26/11/117503

Faster vortex core switching with lower current density using three-nanocontact spin-polarized currents in a confined structure

Hua-Nan Li(李化南), Zhong Hua(华中), Dong-Fei Li(李东飞)
Chin. Phys. B . 2017, 26(1): 017502. **doi:** 10.1088/1674-1056/26/1/017502

Shape-manipulated spin-wave eigenmodes of magnetic nanoelements

Zhang Guang-Fu, Li Zhi-Xiong, Wang Xi-Guang, Nie Yao-Zhuang, Guo Guang-Hua
Chin. Phys. B . 2015, 24(9): 097503. **doi:** 10.1088/1674-1056/24/9/097503

Nonmonotonic effects of perpendicular magnetic anisotropy on current-driven vortex wall motions in magnetic nanostripes

Su Yuan-Chang, Lei Hai-Yang, Hu Jing-Guo
Chin. Phys. B . 2015, 24(9): 097506. **doi:** 10.1088/1674-1056/24/9/097506

Micromagnetic simulation of Sm-Co/*α*-Fe/Sm-Co trilayers with various angles between easy axes and the film plane

Zhang Xi-Chao, Zhao Guo-Ping, Xia Jing, Yue Ming, Yuan Xin-Hong, Xie Lin-Hua
Chin. Phys. B . 2014, 23(9): 097504. **doi:** 10.1088/1674-1056/23/9/097504

Interfacial effect on the reverse of magnetization and ultrafast demagnetization in Co/Ni bilayers with perpendicular magnetic anisotropy*

Zi-Zhao Gong(弓子召)[1,2], Wei Zhang(张伟)[2,3], Wei He(何为)[2], Xiang-Qun Zhang(张向群)[2], Yong Liu(刘永)[1,†], and Zhao-Hua Cheng(成昭华)[2,3,‡]

[1] *State Key Laboratory of Metastable Materials Science & Technology and Key Laboratory for Microstructural Material Physics of Hebei Province, School of Science, Yanshan University, Qinhuangdao* 066004, *China*

[2] *State Key Laboratory of Magnetism and Beijing National Laboratory for Condensed Matter Physics, Institute of Physics, Chinese Academy of Sciences, Beijing* 100190, *China*

[3] *School of Physical Sciences, University of Chinese Academy of Sciences, Beijing* 100190, *China*

(Received 4 February 2018; revised manuscript received 13 March 2018; published online 26 April 2018)

For static magnetic properties of the Co/Ni bilayers, macroscopic hysteresis loops and microscopic magnetic moment distributions have been determined by the object oriented micromagnetic framework (OOMMF). It is found that when the bilayer systems are fully decoupled, the magnetizations of the two phases reverse separately. The coercivity of the bilayers decreases to a valley value sharply with increasing interfacial exchange coupling and then rises slowly to a platform. On the other hand, we have carried out an atomistic simulation for the laser-induced ultrafast demagnetization of the Co/Ni bilayer. A larger damping constant leads to a faster demagnetization as well as a larger degree of demagnetization, which is consistent with the first-principle theoretical results. For the magnetization recovery process, the damping constant has different influences on the recovery time with various peak electron temperatures, which is ignored in previous atomistic simulations as well as the Landau–Liftshit–Bloch (LLB) micromagnetic calculations. Furthermore, as the interfacial exchange coupling increases, the ultrafast demagnetization curves for Co and Ni become coincident, which is a demonstration for the transition from two-phase phenomenon to single-phase phenomenon.

Keywords: micromagnetic simulation, interfacial effect, hysteresis loops, ultrafast demagnetization

PACS: 75.60.Jk, 75.78.–n, 75.70.Cn, 75.78.Cd **DOI:** 10.1088/1674-1056/27/5/057501

1. Introduction

The Co/Ni magnetic multilayered thin films with perpendicular anisotropy have drawn a great deal of attention in the past several decades owing to their applications in the field of magnetic storage and spintronic devices.[1] The properties of interface induced large perpendicular magnetic anisotropy (PMA)[2] can be modified by controllable experimental conditions. The PMA with Ni as the capping layer increases linearly with the annealing temperature. It is in contrast to that in the case of the Pt capping layer.[3] The influence of the layer repetition numbers and film thickness on PMA has been studied by You *et al*.[4] The interfacial effect is very critical for obtaining the high quality thin film, and in turn it can affect both the static and dynamic properties of the bilayers. Up to now, the fast magnetization dynamics in GHz frequency has been discussed widely in Co/Ni systems. For instance, the relationship between Gilbert damping and magneto-crystalline was studied using an all-optical method.[5–7] Also, the dependence of the intrinsic Gilbert damping on the stack number as well as the layer thickness was reported for Co/Ni thin films.[8] However, the ultrafast demagnetization in Co/Ni bilayer on the sub-ps scale is rarely reported, which is helpful for understanding the terahertz emission in such thin films with large PMA.[9]

In this study, the hysteresis loops and magnetic reversal process of a Co/Ni bilayer system were calculated using the object oriented micromagnetic framework (OOMMF), in which the interfacial exchange coupling constant plays a major role. More importantly, we also investigated the interfacial effect on the laser induced ultrafast demagnetization dynamics in the Co/Ni bilayer based on the atomistic spin dynamics model. Our work can open a novel avenue to manipulate the ultrafast demagnetization via the interfacial exchange coupling constant in perpendicular magnetic anisotropic Co/Ni bilayers, and it has an immediate implication for the design of high frequency spintronic devices.

2. Static magnetic properties

2.1. Micromagnetic model

The three-dimensional (3D) micromagnetic calculation of the OOMMF code is based on the Landau–Lifshitz–Gilbert

*Project supported by the National Basic Research Program of China (Grant Nos. 2015CB921403 and 2016YFA0300701), the National Natural Science Foundation of China (Grant Nos. 91622126, 51427801, and 51671212), and the Natural Science Foundation of Hebei Province, China (Grant No. A2015203021).

†Corresponding author. E-mail: ycliu@ysu.edu.cn

‡Corresponding author. E-mail: zhcheng@iphy.ac.cn

© 2018 Chinese Physical Society and IOP Publishing Ltd

dynamic equations[10,11]

$$\frac{\mathrm{d}\boldsymbol{M}}{\mathrm{d}t} = -|\bar{\gamma}|\,\boldsymbol{M}\times\boldsymbol{H}_{\mathrm{eff}} - \frac{|\bar{\gamma}|\,\alpha}{M_{\mathrm{s}}}\boldsymbol{M}\times(\boldsymbol{M}\times\boldsymbol{H}_{\mathrm{eff}}), \quad (1)$$

where $\boldsymbol{M}$ is the magnetization, H_{eff} is the effective field, $\bar{\gamma}$ is the Landau–Lifshitz gyromagnetic ratio, and α is a dimensionless damping constant. The effective field is defined as follows:

$$\boldsymbol{H}_{\mathrm{eff}} = -\mu_0^{-1}\frac{\partial \boldsymbol{E}}{\partial \boldsymbol{M}}. \quad (2)$$

The average energy density E in Eq. (2) is a function of $\boldsymbol{M}$ specified by Brown's equations[12]

$$E = A(r)\left[\frac{\nabla M}{M_{\mathrm{s}}}\right]^2 - K(r)\frac{(\boldsymbol{M}\cdot\boldsymbol{n})^2}{M_{\mathrm{s}}^2} - \mu_0\boldsymbol{M}\cdot\boldsymbol{H} - \frac{1}{2}\mu_0\boldsymbol{H}_{\mathrm{d}}(r)\cdot\boldsymbol{M}, \quad (3)$$

where A and K are the exchange and anisotropy energy constants, respectively, $\boldsymbol{H}$ and $\boldsymbol{H}_{\mathrm{d}}(r)$ are the applied and magnetostatic self-interaction fields, while $M_{\mathrm{s}} = M(r)$ is the spontaneous magnetization. These equations hold for both the Co and Ni phases. The four terms at the right side of Eq. (3) correspond to the exchange energy, the anisotropy energy, the applied field (Zeemam) energy, and the magnetostatic (demagnetization) energy, respectively.

In the 3D simulation carried out by OOMMF, the length and width of both the Co and Ni layers are set as 20 nm. The material is divided into small cells whose length and width are 2.0 nm. The height of each cell is set as 0.1 nm. The applied field varies from 3 T to −3 T in the simulation, starting from a positive saturation state, in which the magnetic moments in each cell are uniformly distributed with the initial magnetization parallel to the applied field.

In this work, both Co and Ni have a strong PMA with the following parameters:[13] $M_{\mathrm{s}}^{\mathrm{Co}} = 1.72$, $M_{\mathrm{s}}^{\mathrm{Ni}} = 0.60$, $K^{\mathrm{Co}} = 6.69\times10^{-24}$ J/atom, $K^{\mathrm{Ni}} = 5.47\times10^{-26}$ J/atom, $A^{\mathrm{Co}} = 6.06\times10^{-21}$ J, and $A^{\mathrm{Ni}} = 2.757\times10^{-21}$ J. The thicknesses of the Co and Ni layers keep constant values of 0.4 nm and 1.6 nm, respectively. Only the exchange interaction between the neighboring region pair is taken into account and the free boundary conditions are chosen. The exchange energy constant between the Co and Ni layers is varied to consider its effect on the magnetization reversal.

2.2. Macroscopic hysteresis and magnetic moment distribution in the film

Figure 1 shows the macroscopic hysteresis loops of the Co/Ni bilayers with various interfacial exchange coupling constants. We can see that some obvious dissimilarities in the hysteresis loops are caused by the varying interfacial exchange coupling constants. When $j_{\mathrm{inter}} = 5\times10^{-21}$ J, corresponding to the case of strong coupling, the hysteresis loop displays a good squareness behavior, indicating that the magnetization of the whole bilayers takes a complete reversal coherently. The underlying magnetization reversal can be illustrated clearly by the 3D magnetization moment distribution shown in Figs. 2(a) and 2(b). We note that, once the applied field is large enough, the orientation of magnetic moment in both Co and Ni changes from positive to negative simultaneously. The loops for $j_{\mathrm{inter}} = 5\times10^{-25}$ J and $j_{\mathrm{inter}} = 0$ J, however, exhibit a kink phenomenon, indicating that the magnetization reversal occurs in two steps. As illustrated in Figs. 2(c) and 2(d), the first step corresponds to the magnetization reversal of the Ni phase which has a smaller switching field and the second one corresponds to the Co phase reversal. For intermediate interfacial exchange energy constant, the squareness of the hysteresis loops is kept well enough, while the critical field of coercivity has a valley value. The interfacial coupling constant also has an important influence in the SmCo/Fe and NdFeB/Fe exchange coupled systems, where the squareness of the hysteresis loop deteriorates with interfacial exchange coupling decreasing.[14–16]

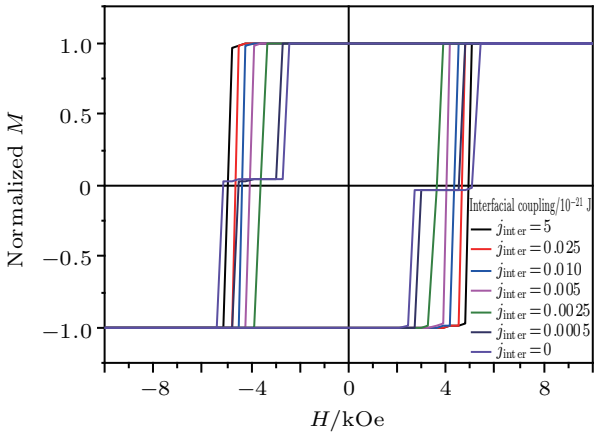


Fig. 1. (color online) Calculated major hysteresis loops of the Co/Ni bilayers with out plane easy axes based on OOMMF with various interface exchange energy constants.

2.3. Critical field

The interfacial exchange coupling constant plays an important role in determining the hysteresis loops, and consequently the intrinsic coercivity. Figure 3 presents the coercivity as a function of the interfacial exchange coupling. The coercivity of the bilayers decreases to a valley value sharply with increasing interfacial exchange coupling and then rises slowly to a platform. The variation of the system's energy barrier with the interfacial exchange coupling constant may contribute to the above relationship. According to the analytical solutions[17] based on the Stoner–Wohlfarth model in exchange-coupled magnets, the energy barrier of the Ni phase increases with the coupling constant, whose magnetocrystalline anisotropy is weak compared with that of the Co phase. In contrast, the energy barrier of Co decreases with the interfacial exchange coupling constant. So a critical interfacial coupling constant exists where the kink in the hysteresis loops disappears and the valley value of coercivity occurs.

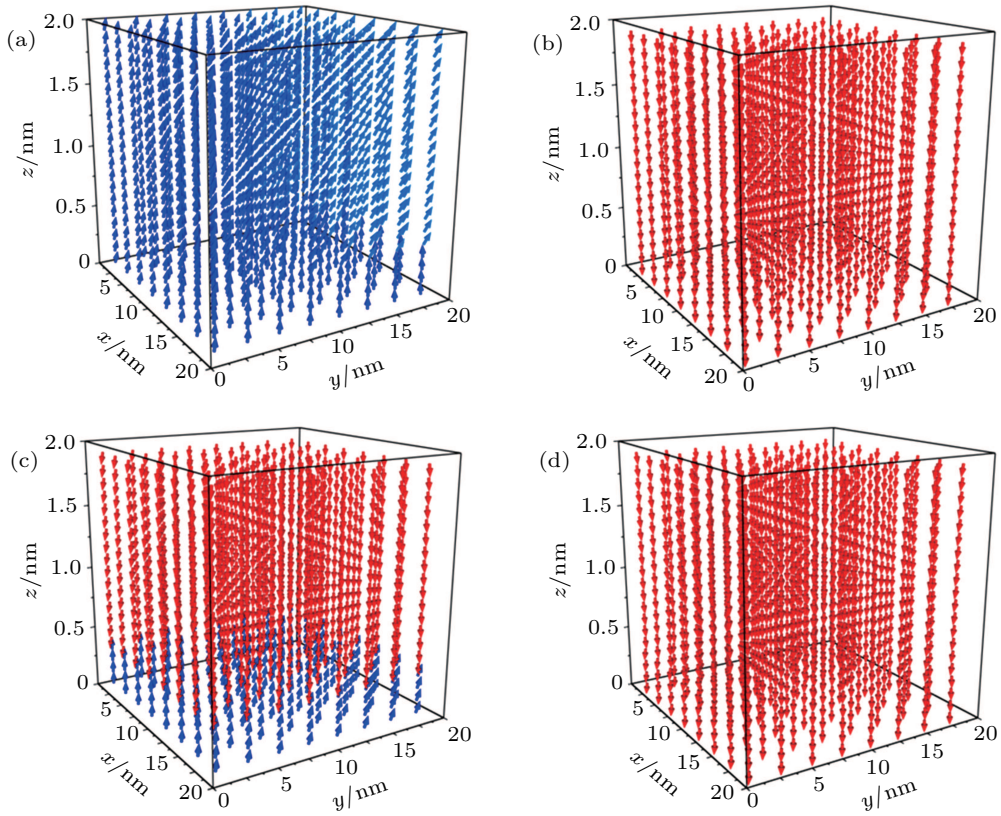


Fig. 2. (color online) 3D evolution of the magnetic moments calculated by OOMMF for Co/Ni bilayers: (a) before coercivity with $j_{\text{inter}} = 6 \times 10^{-21}$ J, (b) after coercivity with $j_{\text{inter}} = 6 \times 10^{-21}$ J, (c) before coercivity with $j_{\text{inter}} = 0$, (d) after coercivity with $j_{\text{inter}} = 0$.

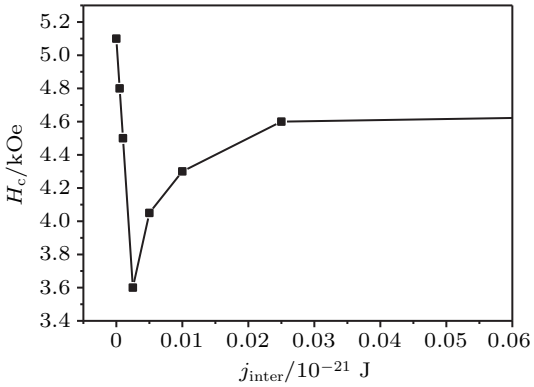


Fig. 3. Calculated coercivity as a function of interfacial exchange energy constant.

3. Dynamic magnetic properties

3.1. Atomistic spin model

The ultrafast demagnetization dynamics is simulated with an atomistic spin model using the Vampire software package.[13,18] In this atomistic simulation, the energetics of the systems are described by an extended Heisenberg spin model with the following form:

$$H = -\sum_{i \neq j} J_{ij} \boldsymbol{S}_i \cdot \boldsymbol{S}_j - k_{\text{u}} \sum_i (\boldsymbol{S}_i \cdot \boldsymbol{e})^2 - \sum_i \mu_{\text{s}} \boldsymbol{S}_i \cdot \boldsymbol{H}_{\text{app}}. \quad (4)$$

The first term is the dominant one called Heisenberg exchange energy, where J_{ij} is the exchange interaction constant between the nearest neighboring two spins $\boldsymbol{S}_i$ and $\boldsymbol{S}_j$. The second term describes the magnetocrystalline anisotropy of the spin, where k_{u} is the uniaxial anisotropy energy per atom. And the last term is the Zeeman energy involving interactions between the system and external applied fields, where μ_{s} is the magnetization moment per atom.

The dynamics of spin systems are determined by the Landau–Liftshit–Gilbert equation with Langevin dynamics

$$\frac{\partial \boldsymbol{S}_i}{\partial t} = -\frac{\gamma}{(1+\lambda^2)} \left[\boldsymbol{S}_i \times \boldsymbol{H}^i_{\text{eff}} + \lambda \boldsymbol{S}_i \times (\boldsymbol{S}_i \times \boldsymbol{H}^i_{\text{eff}}) \right], \quad (5)$$

where γ is the gyromagnetic ratio, and λ is the microscopic damping parameter mainly coming from the intrinsic contributions of spin–electron and spin–lattice interactions. $\boldsymbol{H}^i_{\text{eff}}$ is the net magnetic field on each spin including an additional white noise term[19]

$$\boldsymbol{H}^i_{\text{th}} = \Gamma(t) \sqrt{\frac{2\lambda k_{\text{B}} T}{\gamma \mu_{\text{s}} \Delta t}},$$

where k_{B} is the Boltzmann constant, T is the system temperature, Δt is the integration time step, and $\Gamma(t)$ is the Gaussian white noise term representing the thermal fluctuations on each atomic site. So, the effective field in the above LLG equation with Langevin Dynamics reads

$$\boldsymbol{H}^i_{\text{eff}} = -\frac{1}{\mu_{\text{s}}} \frac{\partial H}{\partial \boldsymbol{S}_i} + \boldsymbol{H}^i_{\text{th}}. \quad (6)$$

The system temperature is calculated from a two-temperature model which couples the spin and electron systems closely and equilibriums with the phonon system in the end. The famous two-temperature model has been widely used in order to understand the laser-induced ultrafast demagnetization dynamics.[20]

3.2. Damping dependence of ultrafast demagnetization

As shown in Fig. 4, a rapid decrease of magnetization takes place on the sub-picosecond timescale. It is consistent with previous experiments,[21] indicating that the macroscopic LLG equation applied at the atomistic level contains the physics of ultrafast demagnetization behavior. The simulations are carried out for Co single layer thin film with λ ranging from 0.01 to 0.25. We note that a larger microscopic damping constant leads to a faster and larger demagnetization. In fact, the microscopic damping parameter λ coming from the local intrinsic contributions (spin–lattice and spin–electron interactions) in the atomistic spin dynamics model, as the bridge between the spins and the heat baths of electrons and phonons, represents the strength of the spin–orbit coupling effect.[22,23] Therefore, it is expected that a larger microscopic damping parameter λ can facilitate the laser induced ultrafast demagnetization as shown in Fig. 4. As the microscopic damping constant λ increases, the demagnetization time τ_{de} declines monotonously.

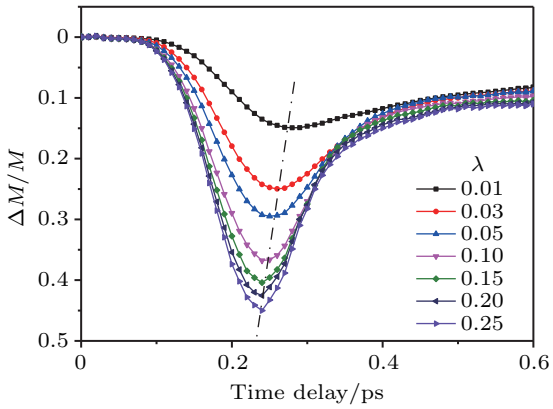


Fig. 4. (color online) Ultrafast demgnetization curves for Co film with various damping constants.

It turns out that λ in the atomistic spin model can be defined by the microscopic spin-flip rate as done in LLB micromagnetic simulations.[24,25] As the material-specific intrinsic spin scattering rate, it is necessary to investigate its influence roughly in a large range of λ as shown in Fig. 5. The largest microscopic damping constant results in a rapid magnetization decay followed by a pronounced recovery process. This value of damping corresponds to that of 3d transition metal with a relatively high spin-flip probability. However, the smallest microscopic damping constant gives rare earth dynamics shown as a slow demagnetization process without any obvious recovery. To some extent, the various microscopic damping constant known as the spin-flip rate in this atomistic simulation defines the diversity of ultrafast demagnetization behaviors compared with the M3TM model.[21]

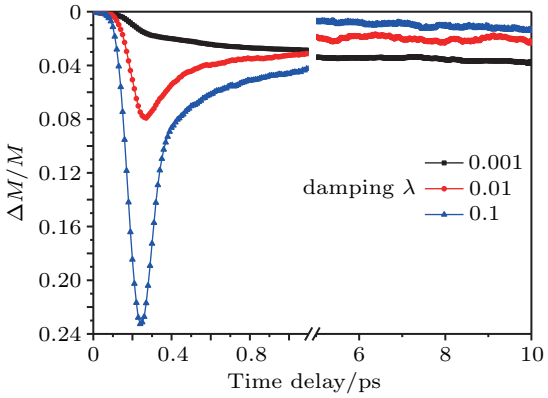


Fig. 5. (color online) Ultrafast demagnetization curves with a large range of microscopic damping constant.

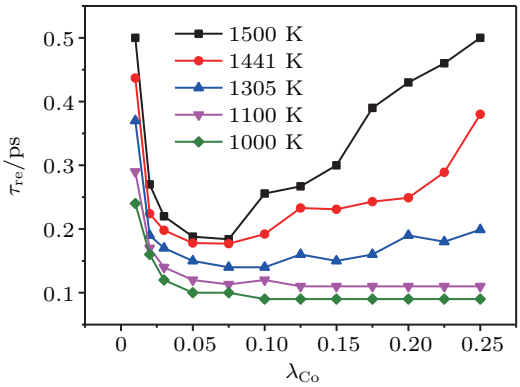


Fig. 6. (color online) Recovery time of Co film as a function of microscopic damping constant with various electron temperatures.

In the ultrafast magnetization dynamics, the recovery time[26] is another critical parameter besides the above demagnetization time and demagnetization state. Figure 6 gives the relationship between the recovery time and microscopic damping constant with various peak electron temperatures. As can be clearly observed, the relationship presents different trends for peak electron temperatures below and above the Curie temperature 1300 K. With microscopic damping constant increasing, the recovery time drops gradually to a constant value for peak electron temperatures below the Curie point, while it decreases to a valley value first and then rises again with the electron temperature exceeding the Curie point. In the atomistic spin dynamics model, the microscopic damping constant can be treated as the coupling strength between the spins and lattice. In this aspect, it can explain the monotonous decreasing relationship for the recovery time and microscopic damping parameter. The stronger coupling strength leads to a faster angular momentum transfer to the lattice, consequently a shorter time to recover the magnetization. However, the magnetization recovery rate also depends on the final magnetic state.[27]

In detail, the recovery of the magnetization will be slowed down with a larger demagnetization. It is based on the interpretation that the magnetic recovery from the demagnetized state takes place via the growth of magnetization which recovers in random directions. The maximum magnetic quenching will be larger with a higher electron temperature as well as a larger microscopic damping constant. Therefore, it is expected that the recovery time shows a non-monotonic behavior with the microscopic damping constant increasing.

3.3. Interfacial exchange coupling dependence of ultrafast demagnetization time

Up to now, we have investigated the effect of interactions among spins, electrons, and lattice in cobalt single layer thin film carefully. Though similar principles still hold for the Co/Ni bilayer system, the effect of the interfacial coupling constant on the ultrafast demagnetization is worth-investigating. In statics, the hysteresis loops present distinct magnetization reversal behaviors with various interfacial coupling. In dynamics, the ultrafast demagnetization curves for the Co and Ni phases in the Co/Ni bilayer on the timescale less than 1 ps are regulated by the interfacial exchange coupling as well. In Fig. 7, the demagnetization curves for Co and Ni coincide with each other in the strong interfacial coupling case, indicating that the bilayer system behaves as an entirety. While the above two curves for Co and Ni separate with each other in the weak interfacial coupling case. It indicates that the interfacial coupling constant between Co and Ni thin layers not only plays a major role in determining the magnetic reversal behaviors, but also in the ultrafast demagnetization dynamics.

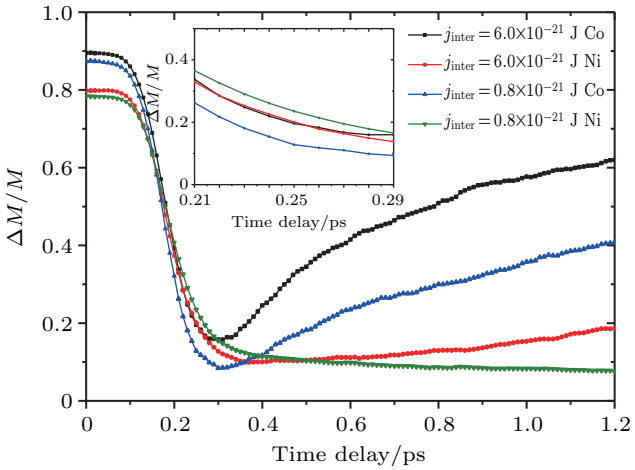


Fig. 7. (color online) Ultrafast demagnetization curves for Co and Ni in Co/Ni bilayers with interfical coupling constant $j_{\text{inter}} = 6.0 \times 10^{-21}$ J and $j_{\text{inter}} = 0.8 \times 10^{-21}$ J. The inset shows the partial enlarged details of the main figure between 0.21 ps to 0.29 ps of time delay.

4. Conclusion

In this study, the static and dynamics properties of Co/Ni bilayers have been studied using 3D micromagnetic simulation and atomistic spin dynamics model, respectively. The coercivity of the bilayers decreases to a valley value sharply with increasing interfacial exchange coupling and then rises slowly to a platform. Also, the interfacial coupling between the Co and Ni layers affects the magnetic reversal in Co/Ni bilayers. The microscopic damping constant in the atomistic spin dynamics domains the ultrafast demagnetization mechanism in Co/Ni bilayers. The recovery time of the magnetization after the laser pulse shows a non-monotonic behavior with the increasing microscopic damping due to the coexistence influence from both the coupling constant between the spin and lattice and the final demagnetization state.

References

[1] Daalderop G H O, Kelly P J and Broeder F J A 1992 *Phys. Rev. Lett.* **68** 682
[2] Ju H L, Li B H, Wu Z F, Zhang F, Liu S and Yu G H 2015 *Acta Phys. Sin.* **64** 097501 (in Chinese)
[3] Yang E, Sokalski V M, Moneck M T, Bromberg D M and Zhu J G 2013 *J. Appl. Phys.* **113** 17C116
[4] You L, Sousa R C, Bandiera S, Rodmacq B and Dieny B 2012 *Appl. Phys. Lett.* **100** 172411
[5] Kato T, Matsumoto Y, Okamoto S, Kikuchi N, Kitakami O, Nishizawa N, Tsunashima S and Iwata S 2011 *IEEE. Trans. Magn.* **47** 10
[6] Song H S, Lee K D, Sohn J W, Yang S H, Parkin S S P, You C Y and Shin S C 2013 *Appl. Phys. Lett.* **102** 102401
[7] Song H S, Lee K D, Sohn J W, Yang S H, Parkin S S P, You C Y and Shin S C 2013 *Appl. Phys. Lett.* **103** 022406
[8] Mizukami S, Zhang X, Kubota T, Naganuma H, Oogane M, Ando Y and Miyazaki T 2011 *Appl. Phys. Express* **4** 013005
[9] Pal S, Polley D, Mitra R K and Barman A 2015 *Solid State Commu.* **221** 50
[10] Donahue M J and Porter D G 1999 *OOMMF user's guide, version* 1.0. *NISTIR* 6376, National Institute of Standards and Technology, Gaithersburg, MD
[11] Zhang W, Zhao G P, Yuan X H and Ye L N 2012 *J. Magn. Magn. Mater.* **324** 4231
[12] Brown W F 1945 *Rev. Mod. Phys.* **17** 15
[13] Evans R F L, Fan W J, Chureemart P, Ostler T A, Ellis M O A and Chantrell R W 2014 *J. Phys.: Condens. Matter* **26** 103202
[14] Sang C X, Zhao G P, Xia W X, Wan X L, Morvan F J, Zhang X C, Xie L H, Zhang J, Du J, Yan A R and Liu P 2016 *Chin. Phys. B* **25** 037501
[15] Deng Y, Zhao G P, Chen L, Zhang H W and Zhou X L 2011 *J. Magn. Magn. Mater.* **323** 535
[16] Deng Y, Zhao G P and Bo N 2011 *Acta Phys. Sin.* **60** 037502 (in Chinese)
[17] Shan Z S, Liu J P, Chakka V M, Zeng H and Jiang J S 2002 *IEEE. Tran. Magn.* **385** 2907
[18] Evans R F L, Ostler T A, Chantrell R W, Radu I and Rasing T 2014 *Appl. Phys. Lett.* **104** 082410
[19] Garcia-Palacios J L and Lazaro F J 1998 *Phys. Rev. B.* **58** 14937
[20] Beaurepaire E, Merle J C, Daunois A and Bigot J Y 1996 *Phys. Rev. Lett.* **76** 4250
[21] Koopmans B, Aeschlimann M, Malinowski G, Longa F D, Steiauf D, Fähnle M, Roth T and Cinchetti M 2010 *Nat. Mater.* **9** 259
[22] Zhang G P and Hübner W 2000 *Phys. Rev. Lett.* **85** 3025
[23] Stohr J and Siegmann H C 2012 *Magnetism: From Fundamentals to Nanoscale Dynamics* 586
[24] Atxitia U and Chubykalo-Fesenko O 2011 *Phys. Rev. B* **84** 144414
[25] Atxitia U and Chubykalo-Fesenko O 2010 *Phys. Rev. B* **81** 174401
[26] Kazantseva N, Nowak U, Chantrell R W, Hohlfeld J and Rebei A 2008 *Europhys. Lett.* **81** 27004
[27] Kazantseva1N, Hinzke1D, Nowak U and Chubykalo-Fesenko O 2007 *Phys. Stat. Sol. (b)* **244** 12